2009 American Control Conference
Hyatt Regency Riverfront, St. Louis, MO, USA
June 10-12, 2009

Dynamic Behavior and Control of a Tubular Solid-Oxide Fuel Cell System

S. Ahmad Hajimolana and Masoud Soroush

Abstract— **A dynamic compartmental model based on first principles is developed for a tubular solid oxide fuel cell system. The model accounts for diffusion processes, inherent impedance, transport (heat and mass transfer) processes, electrochemical processes, anode and cathode activation polarizations, and internal reforming/shifting reactions, among others. Dynamic outlet voltage, current and fuel-cell-tube temperature responses of the cell to step changes in external load resistance and conditions of feed streams are presented. Simulation results show that the fuel cell is a multi-time-scale system; some of the cell output responses exhibit consecutive apparent dominant time constants ranging from about 0.2 ms to about 40 s. They also reveal that the temperature and pressure of the inlet air stream and the temperature of the inlet fuel stream strongly affect the dynamics of the fuel cell system. A simple control system is then implemented to control the fuel cell outlet voltage and cell-tube temperature. The results show that the control system can successfully reject unmeasured step changes (disturbances) in the load resistance, the velocity of the inlet air stream, and the pressure, temperature and velocity of the inlet fuel stream.**

I. INTRODUCTION

Solid oxide fuel cells (SOFCs) are considered to be one of the most advanced designs for mid- to large-scale applications up to 2MW1; they are promising types of fuel cells currently being considered as a power source for automobiles and stationary power plants [2], [3]. Since the electrolyte is a layer of ceramic material with high temperature endurable porous media electrodes, SOFCs can generally operate at high temperature range $(800-1000\,^{\circ}C)$. High operating temperature has some advantages, such as high energy conversion efficiency, flexibility of usable fuel type, and high temperature exhaust gas. Disadvantages include potential thermal fatigue failure of the cell material and sealing under the high temperature and that cell temperature fluctuations induce thermal stress in the cell ceramics. Thus, it is important to operate SOFCs in such a way that the stack temperature remains within a tight design range.

In order to analyze the complicated interactions between the various phenomena occurring inside the cell and to optimize the system performance, there has been significant interest in developing dynamic mathematical models for SOFCs. Dynamic models are especially beneficial for testing control strategies in the development stage of SOFCs. Transport phenomena plays an important role in the SOFC performance. However, it is not clear yet which of the phenomena are significant in a particular design and a given operating region. Dynamic modeling of SOFC can be traced back to Achenbach's work [4], [5], in which the transient cell voltage response to changes in temperature and current density was investigated. More recent studies include [6], [7], [8], [9], [10], [11], [12].

Control of solid oxide fuel cells has also received attention in recent years. Sample studies are as follows. Kandepua et al. [13] showed that the power generated and the cell temperature in a SOFC system can be controlled by manipulating the fuel and air feed flow rates using proportional-integral-derivative (PID) control. Kaneko et al. [14] designed and implemented a power controller on a SOFC model. Chaisantikulwat et al. [15] developed a dynamic model of a SOFC and implemented traditional linear controllers. Sorrentino et al. [16] used a proportional-integral (PI) controller to maintain SOFC temperature variation under a safety-threshold by adjusting the excess air flow rate. Auld et al. [17] used a PID controller to regulate the SOFC voltage across a capacitor by adjusting the SOFC power.

In this paper, a dynamic model based on the first principles is developed and used to study dynamic behavior and control of a SOFC. Its simulation provides a quick insight into the dynamic behavior that one can expect from a typical tubular solid oxide fuel cell. Current, outlet voltage and cell-tube temperature responses to step changes in fuel and air inlet conditions and an external load resistance are calculated using Matlab Simulink. Two completely-decentralized PI controllers are then implemented and simulated to study control of the fuel cell outlet voltage and cell-tube temperature.

The remaining of this article is organized as follows. Section II describes briefly the model development. Section III presents and discusses the numerical simulation results. Section IV focuses on completely-decentralized PI control of the SOFC output voltage and cell-tube temperature. Concluding remarks are presented in Section V.

II. MODEL DEVELOPMENT

The tubular SOFC system under study here is a bank of single tubular solid oxide fuel cells (Figure 1). Each cell has two tubes, an outer tube and an inner tube, as shown in Figure 2. The outer tube is a cell tube. The outer surface of the outer tube is the anode side of the cell, and its inner surface is the cathode side. Between the anode and cathode sides (surfaces) lies the solid oxide electrolyte. The inner tube is an air injection and guidance tube, made of alumina, from which, preheated air is injected into the bottom of cell tube and flows over the cathode surface of the cell tube through

S. A. Hajimolana is with the Department of Chemical Engineering, Azad University of Shahrud, Shahrud, Iran

M. Soroush is with the Department of Chemical and Biological Engineering, Drexel University, Philadelphia, PA 19104, USA

Corresponding author: M. Soroush, ms1@drexel.edu

978-1-4244-4524-0/09/$25.00 ©2009 AACC

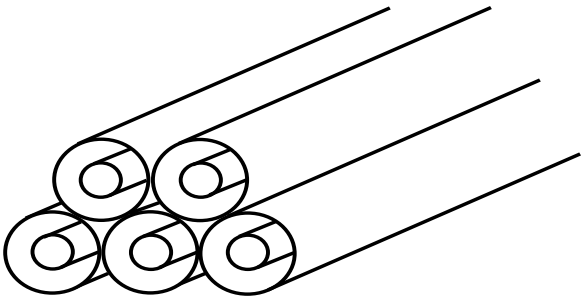

Fig. 1. Tubular SOFC system: a bank of single tubular SOFC cells.

the gap between the injection and cell tubes. Fuel gas flows over the anode surface through the gap among the cell tubes.

A. Electromotive Force of the Fuel Cell: Reversible Voltage

Fuel cell voltage output depends on gas partial pressures and is adversely affected by concentration, activation and ohmic losses (polarizations or irreversibilities). The electromotive force, reversible open-circuit cell voltage, denoted by E_{rev}, is given by Nernst equation:

$$E_{rev} = E_0 + \frac{R_J T_{ct}}{2F} \ln\left(\frac{a_{H_2}^{TPB}\left(a_{O_2}^{TPB}\right)^{0.5}}{a_{H_2O}^{TPB}}\right) \qquad (1)$$

where $a_{H_2O}^{TPB}$, $a_{O_2}^{TPB}$, and $a_{H_2}^{TPB}$ are, respectively, the chemical activities of steam, oxygen and hydrogen at triple phase boundaries (TPB), where the electrochemical reactions take place, and E_0 is the standard cell potential, given by [10]:

$$E_0 = 1.273 - 2.7645 \times 10^{-4} T_{ct}$$

The triple phase boundaries are places where three phases, the ion conducting phase, the electron conducting phase, and the gas phase meet [18]. When the gases are idea, and the vapor pressure of the steam and the standard pressure are equal to one, $a_{H_2}^{TPB} = p_{H_2}^{TPB}$, $a_{O_2}^{TPB} = p_{O_2}^{TPB}$, and $a_{H_2O}^{TPB} = p_{H_2O}^{TPB}$, where $p_{H_2O}^{TPB}$, $p_{O_2}^{TPB}$, and $p_{H_2}^{TPB}$ are, respectively, partial pressures of steam, oxygen and hydrogen at the TPB.

The output voltage of an actual SOFC is less than the voltage given by Eq.(1) due to irreversibilities (polarizations). It is the reversible voltage minus the polarizations (overpotentials). These polarizations (overpotentials) are losses in voltage due to imperfections in materials, microstructure, and design of the fuel cell. Polarizations result from ohmic resistance of oxygen ions conducting through the electrolyte, electrochemical activation barriers at the anode and cathode, and finally concentration polarizations due to inability of gases to diffuse at high rates through the porous anode and cathode. In a SOFC, it is typically most important to focus on the ohmic and concentration polarizations since high operating temperatures experience little activation polarization. However, as the lower limit of SOFC operating temperature ($600°C$) is approached, activation polarization becomes important.

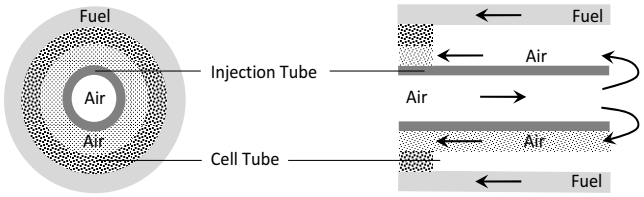

Fig. 2. Front and side views of a single tubular SOFC.

B. Activation Losses (Polarizations)

The activation polarizations are the results of the kinetics involved with the electrochemical reactions. Each reaction has a certain activation barrier that must be overcome in order to proceed, and this barrier leads to the polarization. One can account for the anode and cathode activation polarizations using the Butler–Volmer correlation [10]. Solving the correlation with a transfer coefficient of 0.5 in the high current density regime (where the cell typically operates) leads to:

$$\eta_{act_{ano}} = \frac{R_J T_{ct}}{F} \sinh^{-1}\left(\frac{I}{2I_{0_{ano}}}\right) \qquad (2)$$

$$\eta_{act_{cat}} = \frac{R_J T_{ct}}{F} \sinh^{-1}\left(\frac{I}{2I_{0_{cat}}}\right) \qquad (3)$$

where $I_{0_{ano}}$ and $I_{0_{cat}}$ are the anode and cathode exchange currents, given by [10]:

$$I_{0_{ano}} = 14 \times 10^9 \pi r_{ct_o} L p_{H_2}^{TPB} p_{H_2O}^{TPB} \exp\left(-\frac{E_{act_{ano}}}{R_{kJ} T_{ct}}\right)$$

$$I_{0_{cat}} = 14 \times 10^9 \pi r_{ct_i} L \left(p_{O_2}^{TPB}\right)^{0.25} \exp\left(-\frac{E_{act_{cat}}}{R_{kJ} T_{ct}}\right)$$

This polarization can be modified most easily by microstructural optimization. The area of the TPB is directly related to the electrochemically active area in the cell. The larger the area, the more reactions can occur and thus the less the activation polarization. After deducting the activation losses from the reversible open-circuit cell voltage, E_{rev}, the cell voltage is given by:

$$E = E_0 + \frac{R_J T_{ct}}{2F} \ln\left(\frac{p_{H_2}^{TPB}\left(p_{O_2}^{TPB}\right)^{0.5}}{p_{H_2O}^{TPB}}\right) - \eta_{act_{ano}} - \eta_{act_{cat}} \qquad (4)$$

C. Ohmic Loss: Equivalent Circuit of the Fuel Cell

An approximate equivalent circuit of a SOFC consisting of two internal resistances and one internal capacitance can be found in [11]. According to this equivalent circuit approximation, the cell outlet voltage is governed by:

$$\begin{aligned} \frac{dV_{tl}}{dt} &= \frac{1}{R_{tct} C_{ct}} E - \frac{1}{C_{ct}}\left(\frac{1}{R_{tct}} + \frac{1}{R_{to} + R_{load}}\right) V_{tl} \\ I &= \frac{1}{R_{to} + R_{load}} V_{tl} \\ V_{out} &= R_{load} I \end{aligned} \qquad (5)$$

where R_{to} is the total ohmic resistance in the inherent impedance of the cell, R_{tct} is the total charge transfer

resistance of the cell, C_{ct} is the charge transfer capacitance of the cell, I is the current through the external purely-resistive load, V_{out} is the fuel cell outlet voltage (voltage across the external load), and V_{tl} is the voltage across the total ohmic resistance and the load resistance in series. The rates of consumption of hydrogen and oxygen by the electrochemical reactions to generate an electric current of I are given by: $R_{H_2} = I/(2F)$ and $R_{O_2} = I/(4F)$. The consumption of the reactants is accompanied by the production of water at the following rate: $R_{H_2O} = I/(2F)$. These reaction rates are at TPB.

D. Concentration Losses: Compartmental Modeling

Concentration losses are losses associated with concentration variation of critical species due to mass transport processes. There are usually three sources of loss due to mass transport loss: (i) diffusion between the bulk flows and cell surfaces, (2) diffusion of oxygen ions through the electrolyte (one can also include electron transport), and (3) transport of reactants and products through electrodes.

In order to develop a first-principles model of the SOFC system, a single fuel cell is considered and divided into seven subsystems, as shown in Figure 3:

- Subsystem 1 (SS1): Air inside the injection tube;
- Subsystem 2 (SS2): Injection tube;
- Subsystem 3 (SS3): Air inside the space between the cell and injection tubes; 11
- Subsystem 4 (SS4): Diffusion layer inside the cathode side of the fuel cell tube;
- Subsystem 5 (SS5): Cell tube;
- Subsystem 6 (SS6): Diffusion layer inside the anode side of the fuel cell tube; and
- Subsystem 7 (SS7): Fuel mixture outside (over the anode side) of the cell tube.

The fuel cell model is derived by writing mass, energy and/or momentum conservation equations for each of the seven subsystems. To this end, a number of assumptions are made. Notable among the assumptions are:

- The gas boundary layers are very small relative to the corresponding radius, and therefore, the equations governing the diffusion processes are written in the cartesian coordinates.
- Fluid velocities are average velocity along the radial direction.
- The short length of the fuel cell tube (5 cm) considered here, allows one to assume that partial pressures, temperatures and fluid velocities in each subsystem are uniform in every direction. Specific properties such as conductivities, heat capacities, viscosities, and densities in each subsystem are uniform. Furthermore, outlet partial pressures, temperatures, and velocities are equal to the pressures, temperatures and velocities inside the subsystem. Pipe resistances are negligible. Therefore, no pressure drop in the gases moving inside the fuel cell is caused by pipe resistance.
- Cells external load is a pure resistance.

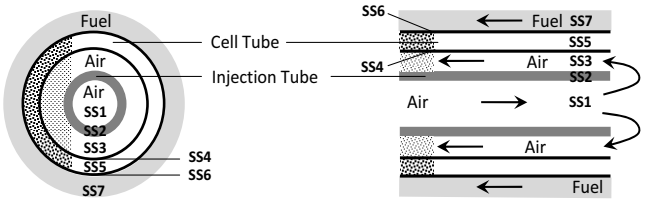

Fig. 3. Division of the single tubular SOFC into five subsystems.

E. Equations Describing SS1–SS7 Dynamics

The equations are obtained by writing the following 19 conservation equations:

- SS1: Total mass balance on air, axial-direction momentum balance on air, energy balance for air
- SS2: Energy balance for the injection tube
- SS3: Total mass balance on air, mass balance on oxygen, axial-direction momentum balance on air, energy balance for air
- SS4: Mass balances on oxygen in the cell-tube cathode-side diffusion layer
- SS5: Energy balance for the cell tube
- SS6: Mass balances on hydrogen and water vapor in the cell-tube anode-side diffusion layer
- SS7: Total mass balance on the fuel, mass balances on hydrogen, methane, water vapor and carbon monoxide, axial-direction momentum balance on the fuel, energy balance for the fuel

These equations together with the model parameter values and relevant correlations can be found in [21].

III. Open-Loop Dynamic Cell Responses

The dynamic model of the SOFC system derived in the previous section has 20 first-order ordinary differential equations, which are integrated numerically using Matlab. The dynamic behavior of the cell-tube temperature and the outlet voltage in response to step changes in the external load resistance and the conditions (pressure, temperature and velocity) of the inlet fuel and air streams are studied. Simulation results show that the fuel cell is a multi-time-scale system, as in the case of other types of fuel cell [19], [20]; some of the cell output responses exhibit consecutive apparent dominant time constants ranging from about 0.2 ms to about 40 s.

Responses to step changes in the external load: Figure 4 depicts the dynamic responses of the fuel cell to $\pm 5\%$ step changes in the external load resistance at time $t = 100$ s. As can be seen, the current and the outlet voltage first change stepwise (show responses with a time constant of 0 s) followed by a slow change with a time constant of about 0.2 ms; this indicates a two-time scale behavior in the voltage and current. The immediate change is a consequence of the direct dependence of the voltage and current on the resistance through the two algebraic equations in Eq.(5). The cell-tube temperature response is significantly slower and has a time constant of about 35 s, as the cell tube has a high heat capacity and mass. The rise in the cell-tube temperature

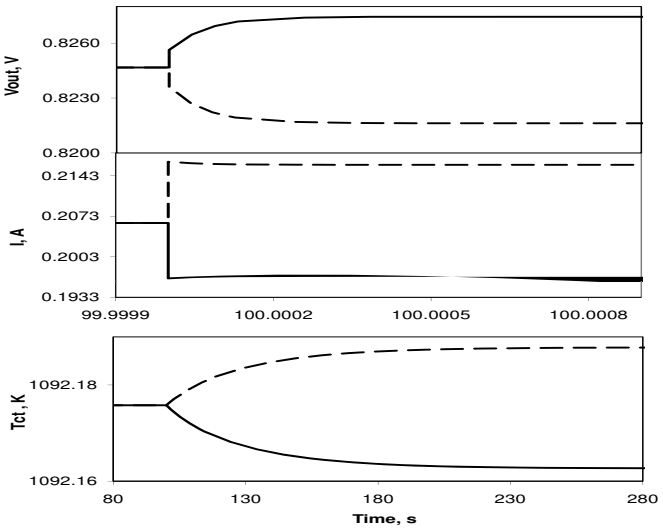

Fig. 4. Open-loop responses to $\pm 5\%$ step changes in the external load.

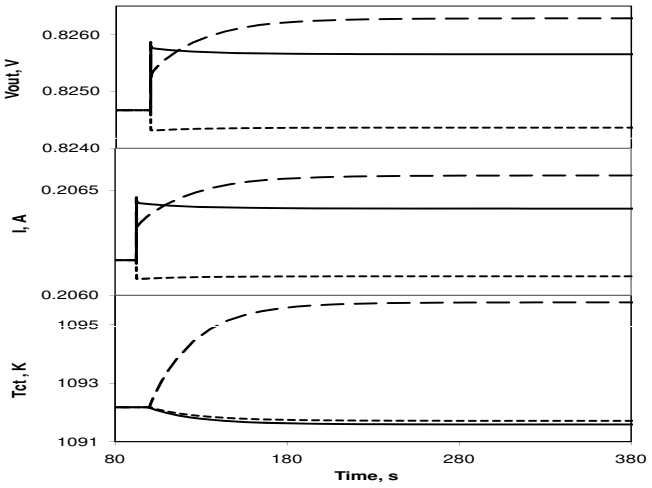

Fig. 5. Open-loop responses to +5% step changes in the inlet fuel pressure (solid line), temperature (dashed line) and velocity (dotted line).

with the decrease in the load resistance is caused by the higher rate of heat release by the electrochemical (oxidation of hydrogen) reaction at the higher current.

Responses to step changes in the inlet fuel conditions: Figure 5 depicts the dynamic responses of the fuel cell to positive 5% step changes in the temperature, pressure and velocity of the inlet fuel stream at time $t = 100\ s$. As can be seen in Figure 5, in response to the step change in the inlet fuel pressure, the current and the outlet voltage first change with a time constant of 25 ms followed by a slow change with a time constant of about 35 s; this indicates a two-time scale behavior in the voltage and current in response to the inlet pressure step change. When the inlet fuel pressure is increased stepwise, the rate of the endothermic reforming reaction increases, leading to the removal of more energy from the cell tube. This explains why the fuel-cell temperature decreases, when the inlet fuel pressure increases. The increase in the rate of the reforming reaction also leads to more production of H_2, which in turn increases the outlet voltage, and subsequently the current.

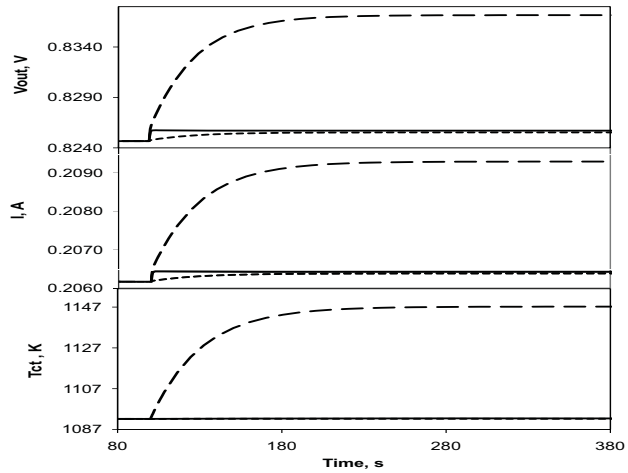

Fig. 6. Open-loop responses to +5% step changes in the inlet air pressure (solid line), temperature (dashed line) and velocity (dotted line).

As can be seen in Figure 5, in response to the step change in the inlet fuel temperature, the current and the outlet voltage first change with a time constant of 2.5 ms followed by a relatively slow change with a time constant of about 25 ms and a slow change with a time constant of about 35 s; this indicates a three-time scale behavior in the voltage and current in response to the inlet temperature step change. A step increase in the inlet fuel velocity leads to an increase in the anode-side film heat-transfer coefficient, causing the removal of more energy from the cell tube, resulting in a decrease in the cell-tube temperature.

Responses to step changes in the inlet air conditions: Figure 6 depicts the dynamic responses of the fuel cell to positive 5% step changes in the temperature, pressure and velocity of inlet air stream at time $t = 100\ s$. A step increase in the inlet air pressure increases the partial pressure of O_2 at TPB, which leads to more production of electrons (higher current and outlet voltage). However, the effects on the current and outlet voltage are not large. This also explains why the increase in the rate of heat release by the reactions is not large.

As can be seen in Figure 6, in response to the step change in the inlet air temperature, the current and the outlet voltage first change with a time constant of $0.4s$ followed by a slow change with a time constant of about 40 s; this indicates a two-time scale behavior in the voltage and current in response to the inlet temperature step change. The effect of the inlet air velocity is not significant. As the velocity increases, the film heat transfer coefficient on the cathode side increases. This higher heat transfer coefficient has little impact on the current, the outlet voltage or the cell-tube temperature. As shown in Figure 6, among the three inlet air conditions, the inlet temperature has the strongest effect on the SOFC temperature and performance dynamically and statically. The inlet air temperature has the strongest effect on the outlet voltage and the cell-tube temperature in terms of steady state gain.

IV. CONTROL OF THE SOFC SYSTEM

An effective control strategy should not steer a SOFC to failure conditions. Common requirements for the operation of a SOFC include: controlling the average stack temperature, ensuring that the fuel-cell temperature is as constant as possible, and maintaining the fuel cell outlet voltage constant. Here, a control system, consisting of two completely-decentralized PI controllers, is implemented is to control the SOFC outlet voltage and cell-tube temperature.

To select the two manipulated inputs that have the strongest effects (in terms of dimensionless steady state gain) on the two controlled outputs around the nominal steady state conditions, $\pm$ 5% step changes in the temperatures, pressures and velocities of the inlet air and fuel streams are made, and the percent of changes in the outlet voltage and the cell-tube temperature are recorded. According to this analysis, the temperature and pressure of the inlet air stream are among the top three inputs in terms of the strength (size) of their steady-state effect on the outlet voltage and the cell-tube temperature. The analysis also suggests that the outlet voltage can be paired with the air inlet pressure and the cell-tube temperature with the air inlet temperature. In other words, the closed-loop system has two feedback loops: Feedback Loop 1 (consisting of PI Controller 1 with the outlet voltage as the controlled output and the inlet air pressure as the manipulated input) and Feedback Loop 2 (consisting of PI Controller 2 with the cell-tube temperature as the controlled output and the inlet air temperature as the manipulated input).

The two PI controllers are first tuned using the internal model control (IMC) guidelines, and the parameters are fine-tuned further by trial and error. Using these approaches, we arrive at: $\tilde{k}_{C_1} = 10$, $\tau_{I_1} = 8\ s$, $\tilde{k}_{C_2} = 2$, and $\tau_{I_2} = 0.1\ s$, where $\tilde{k}_{C_1}$ and τ_{I_1} are the gain and integral time of the PI controller of the air inlet pressure-outlet voltage feedback loop, and $\tilde{k}_{C_2}$, and τ_{I_2} are the gain and integral time of the PI controller of the air inlet temperature-cell tube temperature feedback loop.

To study the effect of load changes on the SOFC performance, a nominal steady state is first found for the SOFC. Under the control system, unmeasured step changes are made in the external load resistance, the inlet fuel pressure, temperature and velocity, and the cell inlet air velocity to investigate the regulatory performance of the control system.

Figure 7 depicts the closed-loop dynamic outlet voltage and cell-tube temperature responses of the fuel cell to $\pm 5\%$ step changes in the external load resistance at time $t = 100\ s$ (two separate simulation runs). As can be seen, the PI controllers are able to reject the disturbances asymptotically. The positive step change initially increases the voltage and decreases the cell-tube temperature. Once the effects of the disturbance appears in the controlled output responses, the simple control system decreases the inlet air pressure and increases the inlet air temperature and push back the controlled outputs to their set-point values.

Figure 8 shows the controlled outputs and the manipulated inputs when three separate (not simultaneous) positive 5% step changes are made at $t = 100\ s$: the inlet fuel pressure from 1 to 1.05 atm, the inlet fuel temperature from 823 to 864 K, and the inlet fuel velocity from 0.927 to 0.973 $m \cdot s^{-1}$. When the fuel inlet pressure is increased from 1 to 1.05 atm, the outlet voltage increases and the cell-tube temperature decreases. Once the control system sees the departures from the setpoint values, it adjusts the manipulated inputs and pushes back the controlled outputs back to their setpoint values. When the inlet fuel temperature increases from 823 to 864 K stepwise, the outlet voltage and the cell-tube temperature increase. The control system then decreases the inlet air pressure and temperature to reject this disturbance asymptotically. When the fuel flow velocity is increased from 0.927 to 0.973 $m \cdot s^{-1}$, the outlet voltage decreases and so does the cell-tube temperature. The control system then increases the inlet air pressure and temperature to reject this disturbance asymptotically. These closed-loop results indicate that the simple control system can reject the three disturbances effectively.

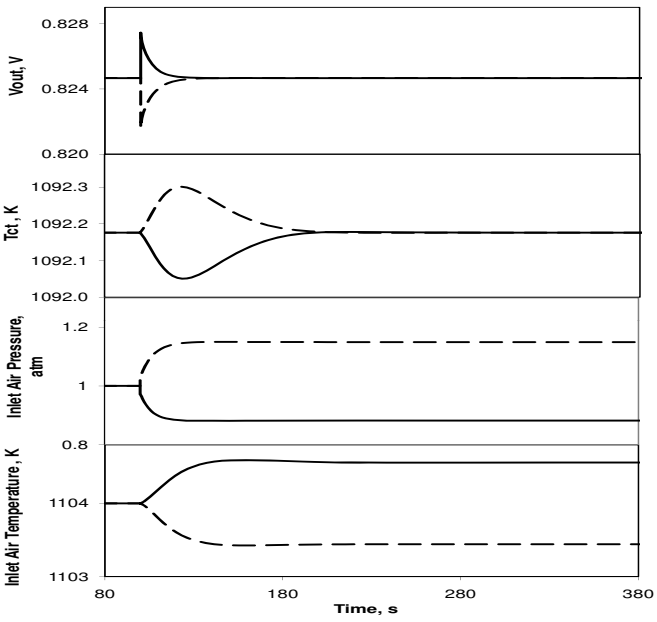

Fig. 7. Closed-loop responses to $\pm 5\%$ step changes in the external load resistance.

Figure 9 depicts the controlled outputs and the manipulated inputs when two separate (not simultaneous) $\pm 5\%$ step changes in the inlet air velocity at $t = 100\ s$. The positive step change leads to increases in the outlet voltage and the cell-tube temperature. The control system then adjusts the inlet air pressure and temperature to reject the disturbance. As seen in Figure 9, the needed adjustments are small. These closed-loop results also indicate that the simple control system can reject the disturbances effectively.

V. CONCLUDING REMARKS

A dynamic model of a tubular solid oxide fuel cell was presented. The model accounts for diffusion processes, inherent impedance, transport (heat and mass transfer) processes, electrochemical processes, anode and cathode activa-

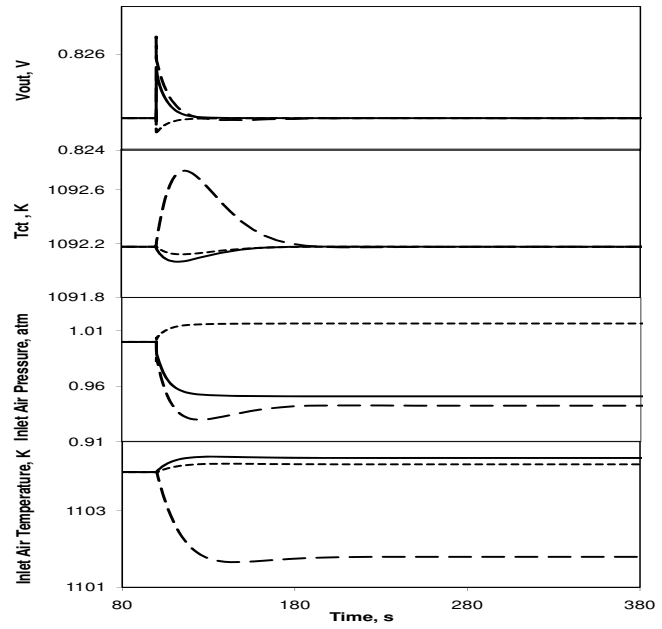

Fig. 8. Closed-loop responses to +5% step changes in the inlet fuel pressure (solid line), temperature (dashed line), and velocity (dotted line).

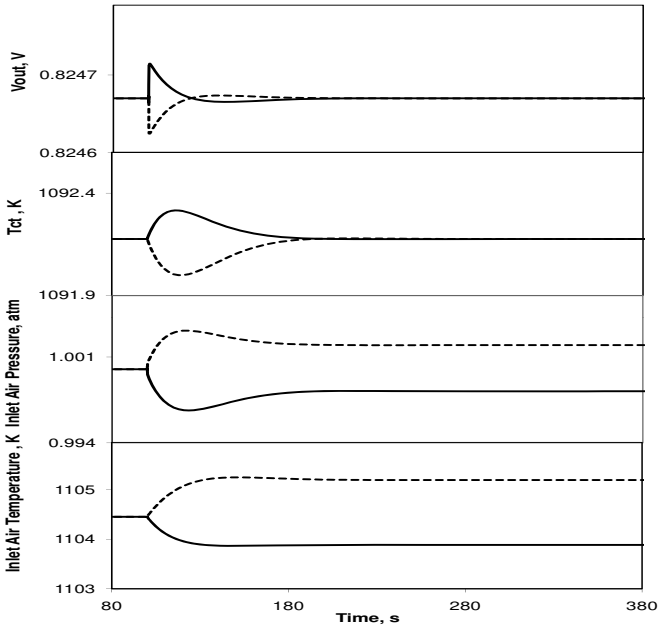

Fig. 9. Closed-loop responses to $\pm 5\%$ step changes in the inlet air velocity.

tion polarizations, and internal reforming/shifting reactions, among others. Dynamic outlet voltage, current and fuel-cell-tube temperature responses of the cell to step changes in external load resistance and conditions of feed streams were presented. Simulations indicated that the transient response of the SOFC was mainly controlled by the temperature dynamics. A nominal steady state was found and chosen as the initial condition for the dynamic simulations. Simulation results also showed that the temperature and pressure of the inlet air stream and the temperature of the inlet fuel stream strongly affect the dynamics of the fuel cell system. They also indicated that temperature of the inlet air stream has the strongest effect on the cell performance, and effects of the inlet air and fuel velocities on the cell response are weaker than those of inlet feed pressures and temperatures. The fuel cell outlet voltage and cell-tube temperature were regulated effectively using a simple control system that manipulates the pressure and temperature of the inlet air stream. The performance of the control system was found satisfactory to reject the unmeasured disturbances.

REFERENCES

[1] Singhal S.C., Advances in solid oxide fuel cell technology, Proc. of the 1998 Fuel Cell Seminar, Courtesy Associates, November (1998).

[2] Srinivasan S., Mosdale R., Stevens P., Yang C. Fuel cells: reaching the era of clean and efficient power generation in the twenty-first century. Annu. Rev. Energy Environ. 24 (1999) 281–328.

[3] Gardner F.J. Thermodynamic processes in solid oxide and other fuel cells. Proc. Inst. Mech. Eng. 211A (1997) 367-380.

[4] Achenbach E. Three-dimensional and time dependent simulation of a planar solid oxide fuel cell stack. J. of Power Sources 49 (1994), 333–348.

[5] Achenbach, E. Response of a solid oxide fuel cell to load change. J. of Power Sources 57 (1995), 105–109.

[6] Morel B., Laurencin J., Bultel Y., Lefebvre-Joud F. Anode-supported sofc model centered on the direct internal reforming. Journal of the Electrochemical Society, 152 (2005), A1382–A1389.

[7] Burt A.C., Celik I.B., Gemmen R.S., Smirnov A.V. A numerical study of cell-to-cell variations in a sofc stack. J. of Power Sources, 126 (2004), 76–87.

[8] Al-Qattan A.M., Chmielewski D.J., Al-Hallaj S., Selman J.R. A novel design for solid oxide fuel cell stacks. Chemical Engineering Science, 59 (2004), 131–137.

[9] Campanari S. Thermodynamic model and parametric analysis of a tubular SOFC module, J. Power Sources 92 (2001) 26–34.

[10] Campanari S., Iora P. Definition and sensitivity analysis of a finite volume sofc model for a tubular cell geometry. Journal of Power Sources, 132 (2004), 113–126.

[11] Qi Y., Huang B., Chuang K.T. Dynamic modeling of solid oxide fuel cell: the effect of diffusion and inherent impedance. Power Sources 150 (2005) 32-47.

[12] Qi Y., Huang B., Jingli L. Dynamic modeling of a finite volume of solid oxide fuel cell: The effect of transport dynamics. Chemical Engineering Science, 61 (2006) 6057–6076.

[13] Kandepua R., Imsland L., Bjarne F.A., Stillerc C., Thorudc B., Bolland O. Modeling and control of a SOFC-GT-based autonomous power system. Energy, 32 (2007), 406-417.

[14] Kaneko T., Brouwer J., Samuelsen G.S. Power and temperature control of fluctuating biomass gas fueled solid oxide fuel cell and micro gas turbine hybrid system. Power Sources, 160 (2006), 316-325.

[15] Chaisantikulwat A., Diaz-Goano C., Meadows E. Dynamic modelling and control of planar anode-supported solid oxide fuel cell. Computers and Chemical Engineering, 32 (2008), 2365–2381.

[16] Sorrentino M., Pianese C., Guezennec Y. A hierarchical modeling approach to the simulation and control of planar solid oxide fuel cells. Journal of Power Sources, 180 (2008), 380–392.

[17] Auld A.E., Mueller F., Smedley K., Samuelsen S., Brouwer J. Applications of one-cycle control to improve the interconnection of a solid oxide fuel cell and electric power system with a dynamic load. Journal of Power Sources. 179 (2008), 155–163.

[18] OHayre R., Barnett D.M., Prinz F.B. The triple phase boundary a mathematical model and experimental investigations for fuel cells. J. of The Electrochemical Society, 152(2) (2005), A439–A444.

[19] Benziger J, Chia JE, Kimball E, Kevrekidis IG. Reaction dynamics in a parallel flow channel PEM fuel cell. Journal Of The Electrochemical Society. 154(8) (2007) B835-B844.

[20] Zenith F., Skogestad S. Control of the mass and energy dynamics of polybenzimidazole-membrane fuel cells. J. of Process Contr. 19 (2009) 415-432.

[21] Hajimolana, S.A., and M. Soroush, Dynamics and control of a tubular solid oxide fuel cell, Ind. Chem. & Eng. Research, in press (2009)